High-Order Mixed RWG Basis Functions for Electromagnetic Applications

Wei Cai, Tiejun Yu, Han Wang, and Yijun Yu

***Abstract*—In this paper, we present an explicit form of high-order mixed Rao–Wilton–Glisson basis functions for electromagnetic (EM) simulation of curved conductor surfaces. Basis functions for combinations of curved triangular and quadrilateral patches can be used. Several applications of EM simulations in multilayered media, such as three-dimensional discontinuities in very large scale integration design, multilayered RF components, and multilayered antennas, are provided to show the feasibility and efficiency of the mixed basis functions.**

***Index Terms*—Electromagnetic scattering, microwave devices, numerical analysis, very large scale integration.**

I. Introduction

THE growth of wireless communication and the increase in clock frequency of microprocessors has made the design of RF/microwave components/subsystems, integrated circuits (ICs), packages, and printed circuit boards (PCBs) ever challenging. It has become indispensable for designer engineers to include the three-dimensional (3-D) parasitic effect via full-wave electromagnetic (EM) analysis during the design process for these applications. Various numerical techniques have been developed to carry out the EM-field simulation, which include the mode-matching method, finite-difference time-domain (FDTD) using Yee scheme [1], or integral-equation formulation [2] with Galerkin-type method of moments (MOM) approximation [3]. Among these numerical techniques, the main advantage of the integral formulation is the reduction of unknowns for problems in 3-D and/or unbounded domains, and its flexibility in handling complex geometry of the scatter surface and the automatic enforcement of Sommerfeld exterior decaying conditions [4] by the construction of proper Green's functions. In this paper, we apply the MOM to solve the mixed-potential integral equation (MPIE) for the extraction of scattering parameters of embedded 3-D RF components, microstrip discontinuities, and multilayer antennas.

Manuscript received July 22, 1999; revised July 17, 2000. This work was supported by the Defense Advanced Research Projects Agency under Grant F49620-96-1-0341 and by the National Science Foundation under Grant CCR-9972251.

W. Cai and Y. Yu are with the Department of Mathematics, University of North Carolina at Charlotte, Charlotte, NC 28223 USA (e-mail: wcai@uncc.edu).

T. Yu was with the Department of Mathematics, University of North Carolina at Charlotte, Charlotte, NC 28223 USA. He is now with the Cadence Company, San Jose, CA 95134 USA.

H. Wang was with the Department of Mathematics, University of North Carolina at Charlotte, Charlotte, NC 28223 USA. He is now with the Enovia Company, Charlotte, NC 28262 USA.

Publisher Item Identifier S 0018-9480(01)05038-4.

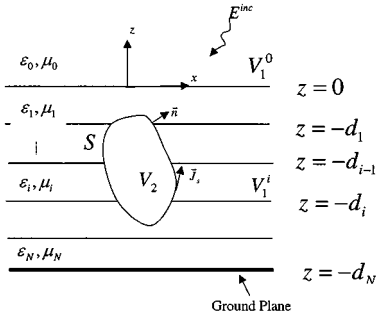

Fig. 1. Multilayer medium with embedded scatter S.

In an MPIE formulation, the EM fields are expressed in terms of surface electrical or magnetic currents on the scatter surface, which is assumed to be embedded in a multilayered exterior medium. The exterior medium considered in this paper is assumed to consist of a planar-layered medium, as shown in Fig. 1. The MPIE-based MOM has the following three important components:

1) derivation and calculation of the multilayered dyadic Green's functions for vector and scalar potentials;
2) representation of surface currents over the scatter surface with the appropriate basis function;
3) solution of the impedance matrix equation resulting from the MOM procedure.

In this paper, we will concentrate on the construction of a new mixed curved or planar triangular and quadrilateral basis function, which can be used to achieve higher order accuracy and efficiency for arbitrary 3-D scattering objects. For the formulation and calculation of a multilayered Green's function, we will use a newly developed fast algorithm [5], which involves a novel mathematical technique for the fast and accurate calculation of Sommerfeld-type integrals arising from the representation of a multilayered dyadic Green's function, the technique can be applied to any number of multilayered medium without a need for surface pole extractions, as in [6] (an improved version has been proposed recently in [7] without surface-wave pole extractions) or the knowledge of a steep-descent path for the Sommerfeld integrals [8]. We will use a direct matrix solver for the solution of the impedance matrix equation.

To represent the current vector field over conductor's surfaces, in many cases, it is important to have a vector basis with continuity of the normal components across the interfaces among adjacent elements. The triangular Rao–Wilton–Glisson (RWG) basis function [9] is the most widely used zeroth-order

basis function. In this paper, we will introduce a newly developed mixed triangular and quadrilateral basis functions, which have the following properties.

1) It is applicable to either curved or flat triangular and/or quadrilateral patches.
2) It can be higher order while the lowest order, over flat triangular patches, reduces to the usual RWG basis functions.
3) The normal components of the current basis are continuous across common interfaces among adjacent patches.

High-order basis functions over triangular patches have been attempted in [10], however, no explicit and easy-to-implement formulations of the basis functions for general high orders have been provided. The MOM using parametric geometry of either triangular or quadrilateral curved patches with first-order basis functions has been used in [11]–[13] for EM scattering calculations. The fact that mixed triangular and quadrilateral basis can be used simultaneously can reduce the total number of unknowns because, in many regions of scatter surfaces, quadrilateral (or rectangle) basis can be used and preferred for better accuracy. Also, a higher order basis function can be useful in reducing the error wherever the fields do not possess singularities like those near edges and corners. The basis function used in this paper is similar to those derived in [14] and can have a variable order of polynomials in different triangles and quadrilaterals.

Section II presents the formulation of the MPIE formulation for scatters embedded in a multilayered medium. Section III provides the construction of the mixed triangular and quadrilateral basis functions. Section IV presents some numerical results with first- and high-order mixed basis functions. Finally, Section V presents the conclusion of this paper.

II. MPIE Formulation

Considered an N-multilayered medium with planer interfaces normal to the z-axis, as depicted in Fig. 1. The interfaces are located at $z = -d_i$, $0 \le i \le N$ and the terminal layer will satisfy various electric- or magnetic-wall boundary conditions. Each of the layers is assumed to be isotropic and lossless or lossy material with permittivity ϵ and permeability μ. Embedded in this multilayered medium is a 3-D conducting object with conductor surface S, whose outward normal is denoted by $\mathbf{n}$. Let $\mathbf{V}_1$ be the multilayered medium outside scatter S and $\mathbf{V}_2$ be the volume inside scatter S. We assume that the EM fields are time harmonic with a time–harmonic factor $\exp(j\omega t)$ being dropped. If the scatter is impacted by an incident wave $\mathbf{E}^{\text{inc}}$, we have the following MPIE [15] for the surface current $\mathbf{J}_s$

$$\mathbf{n}\times j\omega\mu\left[-\int_S \overline{\overline{G}}_A\cdot\mathbf{J}_s\,ds+\nabla\cdot\int_S\frac{1}{k^2}\nabla\overline{\overline{G}}_A\cdot\mathbf{J}_s\,ds\right]=\mathbf{n}\times Z_s\mathbf{J}_s-\mathbf{n}\times\mathbf{E}^{\text{inc}} \quad (1)$$

where $\overline{\overline{G}}_A$ is the dyadic Green's function for the vector potential $\mathbf{A}$, Z_s is the surface impedance, and $k^2=\omega^2\epsilon\mu$.

In our computation, we have chosen the formulation type C described in [16] for the definition of the dyadic Green's function $\overline{\overline{G}}_A$, which has the following modified expression:

$$\overline{\overline{G}}_A=(\hat{x}\hat{x}+\hat{y}\hat{y})G_A^{xx}+\hat{z}\hat{z}G_A^{zz}+\hat{x}\hat{z}G_A^{xz}+\hat{y}\hat{z}G_A^{yz}+\hat{z}\hat{x}G_A^{zx}+\hat{z}\hat{y}G_A^{zy}. \quad (2)$$

The details for the fast calculation of each components in (2) can be found in [16].

For an open perfect-electric-conductor (PEC) scatter, (1) will guarantee an unique solution. However, for a closed PEC scatter, the solution of (1) is not unique at a certain frequency corresponding to the resonant frequency of the cavity inside the scatter. A combined integral-equation approach will be able to address the interior resonance problem [17].

III. Mixed Current Basis Functions

In applying a Galerkin procedure to form a MOM matrix [3], test functions $\mathbf{J}_{s,j}$ will be multiplied to (1) and integrated over the surface S. In order to transfer the ∇ operator in the second term in (1) (the scalar potential term) to the test function $\mathbf{J}_{s,j}$ via integration by parts, normal continuity of the test function $\mathbf{J}_{s,j}$ is needed across the common interface of triangular and quadrilateral/or triangular patches. In this section, we will present such current basis functions; the normal continuity of the current basis functions is the key property of the popular RWG basis functions, which insure no accumulation of charges across the element interfaces. In the following, we will give the formulation of a higher order extension of the usual RWG basis over arbitrary curved patches. Similar higher order basis functions have been discussed in [14]. However, in this paper, we will use hiearchical polynomials as the building blocks for the higher order RWG basis functions.

Let S be a curved triangle or quadrilateral surface in $\mathbb{R}^3$, and S is parameterized by $\mathbf{x}=\mathbf{x}(u_1,u_2)$, $(u_1,u_2)\in T_0$ if S is a triangular patch or $\mathbf{x}=\mathbf{x}(u_1,u_2)$, $(u_1,u_2)\in\Omega_0$ if S is a quadrilateral patch. Here, T_0 is a standard reference triangle in Fig. 2 and Ω_0 is a standard reference square in Fig. 3.

Tangential Vectors: $\partial_i\mathbf{x}\ i=1,2$ are defined as

$$\partial_i\mathbf{x}=\frac{\partial\mathbf{x}}{\partial u_i},\qquad i=1,2 \quad (3)$$

and, for convenience, we also define for triangle patches

$$\partial_3\mathbf{x}=\partial_1\mathbf{x}-\partial_2\mathbf{x}.$$

and $\{g_{\mu\nu}\}$ as the covariant tensor

$$g_{\mu\nu}=\frac{\partial\mathbf{x}}{\partial u_\mu}\cdot\frac{\partial\mathbf{x}}{\partial u_\nu},\qquad 1\le\mu,\nu\le 2. \quad (4)$$

The determinant of $\{g_{\mu\nu}\}$ is denoted by

$$g=\det\{g_{\mu\nu}\}=g_{11}g_{22}-g_{12}^2=\|\partial_1\mathbf{x}\times\partial_2\mathbf{x}\|^2. \quad (5)$$

A. Hierarchical Polynomial Basis over Triangle T_0

Let T_0 be the reference triangle with vertices a, b, c in Fig. 2, we group polynomials of order M into the three modes of: 1) vertex; 2) edge; and 3) internal, as in [18].

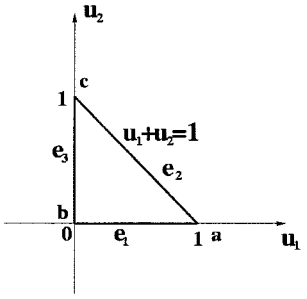

Fig. 2. Reference triangle T_0.

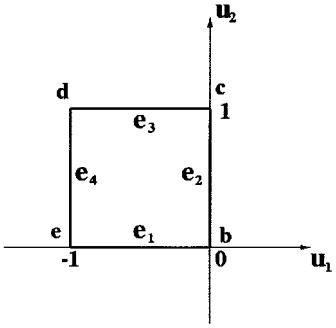

Fig. 3. Reference rectangle Ω_0.

- Vertex modes

$$g_a(u_1, u_2) = u_1$$
$$g_b(u_1, u_2) = 1 - u_1 - u_2$$
$$g_c(u_1, u_2) = u_2. \tag{6}$$

Each vertex mode will take value 1 at one vertex and 0 at the other two vertices.

- Edge modes for $2 \le l \le M$

$$g_l^{ab}(u_1, u_2) = g_a g_b p_{l-2}(g_b - g_a)$$
$$g_l^{bc}(u_1, u_2) = g_b g_c p_{l-2}(g_c - g_b)$$
$$g_l^{ca}(u_1, u_2) = g_c g_a p_{l-2}(g_a - g_c) \tag{7}$$

where $p_l(\xi)$, $\xi \in [-1, 1]$ is the lth order Legendre polynomial.

Each edge mode is only nonzero along one edge of the triangle T_0.

- Internal modes for $0 \le k + l \le M - 3$

$$g_{l,k}^{\text{int}}(u_1, u_2) = g_a g_b g_c p_k(2g_c - 1) p_l(g_b - g_a).$$

Each of the internal mode will vanish over all edges of T_0.

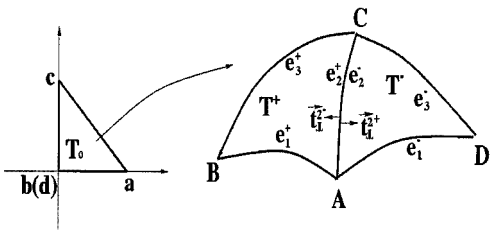

Fig. 4. Curved triangular and triangular patches.

B. Hierarchical Polynomials over Rectangle Ω_0

Let Ω_0 be the reference rectangle with vertices b, c, d, e in Fig. 3. We group polynomials of order M over Ω_0 into the following three modes: 1) vertex; 2) edge; and 3) internal [18].

- Vertex modes

$$N_b(u_1, u_2) = (1 + u_1)(1 - u_2)$$
$$N_c(u_1, u_2) = (1 + u_1)u_2$$
$$N_d(u_1, u_2) = -u_1 u_2$$
$$N_e(u_1, u_2) = -u_1(1 - u_2). \tag{8}$$

Each vertex mode will take value 1 at one vertex and 0 at the other three vertices.

- Edge modes for $2 \le l \le M$

$$N_l^{eb}(u_1, u_2) = (1 - u_2)\phi_l(2u_1 + 1)$$
$$N_l^{bc}(u_1, u_2) = (1 + u_1)\phi_l(2u_2 - 1)$$
$$N_l^{cd}(u_1, u_2) = u_2\phi_l(2u_1 + 1)$$
$$N_l^{de}(u_1, u_2) = -u_1\phi_l(2u_2 - 1) \tag{9}$$

and

$$\phi_l(\xi) = \frac{1}{4}(1 - \xi^2)p_{l-2}(\xi). \tag{10}$$

Each edge mode is only nonzero along one edge of the rectangle Ω_0.

- Internal modes for $2 \le k, l \le M$

$$N_{l,k}^{\text{int}}(u_1, u_2) = \phi_l(2u_1 + 1)\phi_k(2u_2 - 1). \tag{11}$$

Each of the internal mode will vanish over all edges Ω_0.

C. Triangular and Triangular Patches Matching

Consider the two curved triangular patches T^+ and T^- with a common interface AC with length ℓ in Fig. 4. Let T^+ and T^- be parameterized, respectively, by

$$\mathbf{x} = \mathbf{x}^+(u_1, u_2): T_0 \to T^+ \tag{12}$$
$$\mathbf{x} = \mathbf{x}^-(u_1, u_2): T_0 \to T^-. \tag{13}$$

We assume that the interface AC in both T^+ and T^- is parameterized by $u_1 + u_2 = 1$ and is labeled as side e_2^+ in T^+ and side e_2^- in T^-.

Following [14], high-order basis functions with continuous normal components are constructed.

- RWG basis

If we assume that the normal component of the current basis function remains constant along the edge AC in the case of flat triangles, we have

$$\mathbf{f}(\mathbf{x}) = I_n \begin{cases} \dfrac{l}{\sqrt{g^+}}\Big(g_A(u_1, u_2)\partial_1\mathbf{x} + g_C(u_1, u_2)\partial_2\mathbf{x}\Big), \\ \qquad \text{if } \mathbf{x} = \mathbf{x}^+(u_1, u_2) \in T^+ \\ \dfrac{l}{\sqrt{g^-}}\Big(-g_A(u_1, u_2)\partial_1\mathbf{x} - g_C(u_1, u_2)\partial_2\mathbf{x}\Big), \\ \qquad \text{if } \mathbf{x} = \mathbf{x}^-(u_1, u_2) \in T^- \end{cases} \tag{14}$$

and for flat triangle patches, we have in T^+

$$\begin{aligned} \mathbf{x} &= \mathbf{x}^+(u_1, u_2) \\ &= g_A(u_1, u_2)\mathbf{x}_A + g_B(u_1, u_2)\mathbf{x}_B + g_C(u_1, u_2)\mathbf{x}_C \end{aligned} \tag{15}$$

$$\begin{aligned} \partial_1\mathbf{x} &= \mathbf{x}_A - \mathbf{x}_B \\ \partial_2\mathbf{x} &= \mathbf{x}_C - \mathbf{x}_B \end{aligned} \tag{16}$$

and in T^-

$$\begin{aligned} \mathbf{x} &= \mathbf{x}^-(u_1, u_2) \\ &= g_A(u_1, u_2)\mathbf{x}_A + g_D(u_1, u_2)\mathbf{x}_D + g_C(u_1, u_2)\mathbf{x}_C \end{aligned} \tag{17}$$

where $g_D(u_1, u_2) = g_B(u_1, u_2)$

$$\begin{aligned} \partial_1\mathbf{x} &= \mathbf{x}_A - \mathbf{x}_D \\ \partial_2\mathbf{x} &= \mathbf{x}_C - \mathbf{x}_D. \end{aligned} \tag{18}$$

Thus, we have the RWG basis function

$$\mathbf{f}(\mathbf{x}) = I_n \begin{cases} \dfrac{l}{2A^+}(\mathbf{x} - \mathbf{x}_B), & \text{if } \mathbf{x} = \mathbf{x}^+(u_1, u_2) \in T^+ \\ -\dfrac{l}{2A^-}(\mathbf{x} - \mathbf{x}_D), & \text{if } \mathbf{x} = \mathbf{x}^-(u_1, u_2) \in T^- \end{cases} \tag{19}$$

where A^+ and A^- are the areas of triangles T^+ and T^-, respectively.

The unknown for each edge AC is just I_n.

- First-order basis

In this case, we allow the normal component of the current basis function to vary along the edge

$$\mathbf{f}(\mathbf{x}) = \begin{cases} \dfrac{l}{\sqrt{g^+}}\Big(I_n^a g_A(u_1, u_2)\partial_1\mathbf{x} + I_n^c g_C(u_1, u_2)\partial_2\mathbf{x}\Big), \\ \qquad \text{if } \mathbf{x} = \mathbf{x}^+(u_1, u_2) \in T^+ \\ \dfrac{l}{\sqrt{g^-}}\Big(-I_n^a g_A(u_1, u_2)\partial_1\mathbf{x} - I_n^c g_C(u_1, u_2)\partial_2\mathbf{x}\Big), \\ \qquad \text{if } \mathbf{x} = \mathbf{x}^-(u_1, u_2) \in T^-. \end{cases} \tag{20}$$

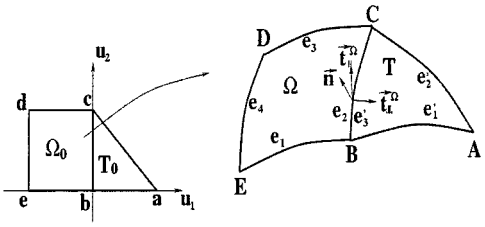

Fig. 5. Curved triangular and quadrilateral patches.

The unknowns for each edge AC are I_n^a, I_n^c.

- Second-order basis

$$\mathbf{f}(\mathbf{x}) = \begin{cases} \dfrac{l}{\sqrt{g^+}}\Bigg\{\Bigg[I_n^a g_A(u_1, u_2) + \dfrac{I_n^{(2)} - \tilde{I}_t^{(2)}}{2} g_2^{e_2^+}(u_1, u_2)\Bigg]\partial_1\mathbf{x} \\ \qquad + \Bigg[I_n^c g_C(u_1, u_2) + \dfrac{I_n^{(2)} + \tilde{I}_t^{(2)}}{2} g_2^{e_2^+}(u_1, u_2)\Bigg]\partial_2\mathbf{x}\Bigg\}, \\ \qquad \text{if } \mathbf{x} = \mathbf{x}^+(u_1, u_2) \in T^+ \\ \dfrac{l}{\sqrt{g^-}}\Bigg\{\Bigg[-I_n^a g_A(u_1, u_2) + \dfrac{-I_n^{(2)} - \hat{I}_t^{(2)}}{2} g_2^{e_2^-}(u_1, u_2)\Bigg]\partial_1\mathbf{x} \\ \qquad + \Bigg[-I_n^c g_C(u_1, u_2) + \dfrac{-I_n^{(2)} + \hat{I}_t^{(2)}}{2} g_2^{e_2^-}(u_1, u_2)\Bigg]\partial_2\mathbf{x}\Bigg\}, \\ \qquad \text{if } \mathbf{x} = \mathbf{x}^-(u_1, u_2) \in T^- \end{cases} \tag{21}$$

where $e_2^+ = e_2^- = ca$. The unknowns for each edge AC are I_n^a, I_n^c, $I_n^{(2)}$, $\hat{I}_t^{(2)}$, and $\tilde{I}_t^{(2)}$.

Higher order current basis functions can be found in the Appendix.

D. Triangular and Quadrilateral Patches Matching

Consider a curved quadrilateral patch Ω and a curved triangular patch T, which are parameterized separately by the two mapping $\mathbf{x}_i(u_1, u_2)$, $i = 1, 2$, i.e.,

$$\begin{aligned} &\mathbf{x}_1(u_1, u_2): \Omega_0 \to \Omega, \qquad (u_1, u_2) \in \Omega_0 \\ &\mathbf{x}_2(u_1, u_2): T_0 \to T, \qquad (u_1, u_2) \in T_0. \end{aligned} \tag{22}$$

The edges of Ω and T are labeled as shown in Fig. 5. The common interface is BC, which is parameterized by $u_1 = 0$. Again, we have the following current basis functions with continuous normal components across the common interface BC.

- Mixed RWG basis

If we assume that the normal component of the current basis function remains constant along the edge BC in case of flat triangular and quadrilateral patches, we have

$$\mathbf{f}(\mathbf{x}) = I_n \begin{cases} \dfrac{l}{\sqrt{g^{\Omega}}}\Big[N_B(u_1, u_2) + N_C(u_1, u_2)\Big]\partial_1\mathbf{x}, \\ \qquad \text{if } \mathbf{x} = \mathbf{x}_1(u_1, u_2) \in \Omega \\ -\dfrac{l}{\sqrt{g^{T}}}\Big[-\big(g_B(u_1, u_2) + g_C(u_1, u_2)\big)\partial_1\,\mathbf{x} \\ \qquad\qquad + g_C(u_1, u_2)\partial_2\mathbf{x}\Big], \\ \qquad \text{if } \mathbf{x} = \mathbf{x}_2(u_1, u_2) \in T. \end{cases} \tag{23}$$

For flat triangular and quadrilateral patches, $\sqrt{g^T} = 2A^T$, A^T denotes the area of T. In Ω

$$\begin{aligned} \partial_1\mathbf{x} &= \partial_1\mathbf{x}_1 = (1-u_2)(\mathbf{x}_B - \mathbf{x}_E) + u_2(\mathbf{x}_C - \mathbf{x}_D) \\ \partial_2\mathbf{x} &= \partial_2\mathbf{x}_1 = -u_1(\mathbf{x}_D - \mathbf{x}_E) + (1+u_1)(\mathbf{x}_C - \mathbf{x}_B) \end{aligned} \tag{24}$$

and in T

$$\begin{aligned} \partial_1\mathbf{x} &= \partial_1\mathbf{x}_2 = \mathbf{x}_A - \mathbf{x}_B \\ \partial_2\mathbf{x} &= \partial_2\mathbf{x}_2 = \mathbf{x}_C - \mathbf{x}_B \\ \partial_3\mathbf{x} &= \partial_3\mathbf{x}_2 = \partial_1\mathbf{x}_2 - \partial_2\mathbf{x}_2 = \mathbf{x}_A - \mathbf{x}_C \end{aligned} \tag{25}$$

thus, we have the mixed RWG basis function

$$\mathbf{f}(\mathbf{x}) = I_n \begin{cases} \dfrac{l}{\sqrt{g^{\Omega}}}(1+u_1)\Big[(1-u_2)(\mathbf{x}_B - \mathbf{x}_E) \\ \qquad\qquad + u_2(\mathbf{x}_C - \mathbf{x}_D)\Big], \\ \qquad \text{if } \mathbf{x} = \mathbf{x}_1(u_1, u_2) \in \Omega \\ -\dfrac{l}{2A^T}(\mathbf{x} - \mathbf{x}_A), \\ \qquad \text{if } \mathbf{x} = \mathbf{x}_2(u_1, u_2) \in T. \end{cases} \tag{26}$$

The unknown for each edge BC is just I_n.

- Mixed first-order basis

$$\mathbf{f}(\mathbf{x}) = \begin{cases} \dfrac{l}{\sqrt{g^{\Omega}}}\Big[I_n^b N_B(u_1, u_2) + I_n^c N_C(u_1, u_2)\Big]\partial_1\mathbf{x}, \\ \qquad \text{if } \mathbf{x} = \mathbf{x}_1(u_1, u_2) \in \Omega \\ \dfrac{l}{\sqrt{g^{T}}}\Big[I_n^b g_B(u_1, u_2)\partial_1\mathbf{x} + I_n^c g_C(u_1, u_2)\partial_3\mathbf{x}\Big], \\ \qquad \text{if } \mathbf{x} = \mathbf{x}_2(u_1, u_2) \in T. \end{cases} \tag{27}$$

The unknowns for each edge BC are

$$I_n^b,\ I_n^c. \tag{28}$$

- Second-order basis

$$\mathbf{f}(\mathbf{x}) = \begin{cases} \dfrac{l}{\sqrt{g^{\Omega}}}\Bigg\{\Big[I_n^b N_B(u_1, u_2) + I_n^c N_C(u_1, u_2) \\ \qquad + I_n^{(2)} N_2^{e_2}(u_1, u_2) \\ \qquad + \gamma_{22}^1 N_{22}^{\text{int}}(u_1, u_2)\Big]\partial_1\mathbf{x} \\ \qquad + \Big[\hat{I}_t^{(2)} N_2^{e_2}(u_1, u_2) \\ \qquad\qquad + \gamma_{22}^2 N_{22}^{\text{int}}(u_1, u_2)\Big]\partial_2\mathbf{x}\Bigg\}, \\ \qquad \text{if } \mathbf{x} = \mathbf{x}_1(u_1, u_2) \in \Omega \\ \dfrac{l}{\sqrt{g^{T}}}\Bigg\{\Big[I_n^b g_B(u_1, u_2) \\ \qquad + \dfrac{I_n^{(2)} - \tilde{I}_t^{(2)}}{2} g_2^{e_3'}(u_1, u_2)\Big]\partial_1\mathbf{x} \\ \qquad + \Big[I_n^c g_C(u_1, u_2) \\ \qquad\qquad + \dfrac{I_n^{(2)} + \tilde{I}_t^{(2)}}{2} g_2^{e_3'}(u_1, u_2)\Big]\partial_3\mathbf{x}\Bigg\}, \\ \qquad \text{if } \mathbf{x} = \mathbf{x}_2(u_1, u_2) \in T \end{cases} \tag{29}$$

where $e_2 = e_3' = BC$.

The unknowns for each edge BC are I_n^b, I_n^c, $I_n^{(2)}$, $\hat{I}_t^{(2)}$, $\tilde{I}_t^{(2)}$, and the unknowns for each quadrilateral are γ_{22}^1, γ_{22}^2.

Higher order current basis functions can be found in the Appendix.

IV. Results and Discussions

Four numerical examples will be presented here to show the advantages of the mixed basis function, and another example will be presented to show the better accuracy of higher order basis functions for the scattering of a 3-D PEC sphere.

S-parameters are the most often used network parameters to be measured at high frequencies. It is also easy to capture the resonant frequency from an S-parameter. After current distribution on the surface of the circuit has been obtained, a deembedding method [19] is used to extract the S-parameters. Three test examples will be presented to demonstrate the capability of the mixed current basis.

A. Test 1—Two Striplines Connected by a Via

The first example is depicted in Fig. 6, which shows a two-layer structure with two ports: two strip lines connected with a cylindrical via. Fig. 7 shows a pure triangular mesh. At the two ports of the circuit, two embedding arms with length greater than 1/4 wavelength are also discretized by triangles and rectangles, respectively. The following table shows the computed results, where "RWG" signifies a pure triangular mesh, "M-RWG" signifies a mixed mesh (triangles and rectangles), and "Structure"

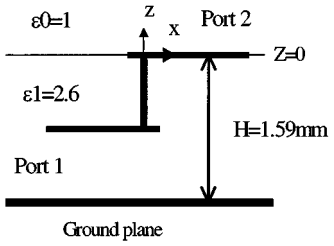

Fig. 6. Geometry of the two strip lines connected by a via with diameter $d = 0.08485$ mm. Both of the lines have a width of $b = 2.4$ mm and a length of $a = 4.8$ mm. Port 1 defined by two points (unit mm): $(-3.6, -1.2, -0.795)$, $(-3.6, 1.2, -0.795)$. Port 2 defined by two points: $(3.6, -1.2, 0)$, $(3.6, 1.2, 0)$.

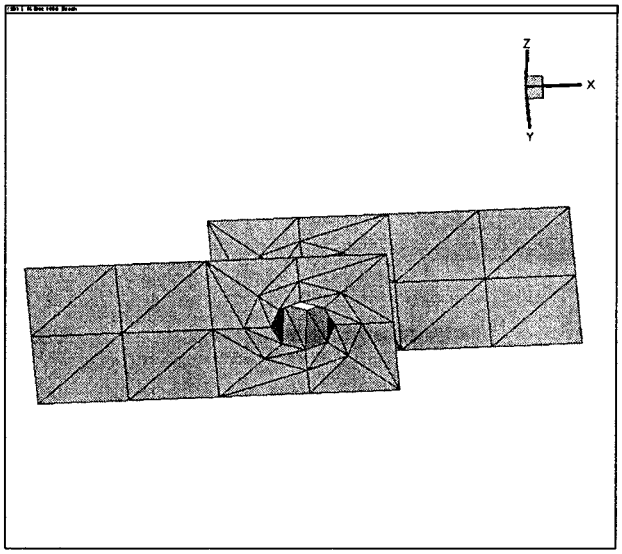

Fig. 7. Two strip lines connected by a via are discretized by pure triangles.

is the circuit itself, while "Embed arm" is the two embedding arms. Mesh points, number of unknowns, memory requirement, and CPU time associated with the matrix solver by LU decomposition are all listed in Table I. Fig. 8 also shows the S-parameters obtained by the two meshes. A result with a pure triangular mesh using Ansoft Inc.'s, Pittsburgh, PA, Maxwell is also included for comparison.

B. Test 2—Multilayer Bandpass Filter

The second example is shown in Fig. 9, which is a complicated bandpass filter with 28 vias embedded in a 23-layer medium, provided by National Semiconductor Inc., Santa Clara, CA, for wireless communication applications. As shown in this figure, a mixed mesh is used to discretize the filter conductor surface and the MOM is used. In Fig. 10, the S_{12}-parameters at the ports have been efficiently calculated and compared well with the experimental measurement by National Semiconductor Inc.

C. Test 3—Multilayer Wide-Band Antenna

The third example is a multilayer wide-band antenna, as shown in Fig. 11. Results with rectangular and triangular meshes agree very well.

TABLE I
COMPARISON OF MEMORY AND CPU TIME FOR RWG AND M-RWG BASIS FUNCTIONS

Compared term		RWG	M-RWG
Mesh No.	Structure	96	80
	Embed arm	80	40
	Total	176	120
Unknown No.	Structure	132	116
	Embed arm	100	60
	Total	232	176
Memory		100%	57.55%
CPU time		100%	43.65%

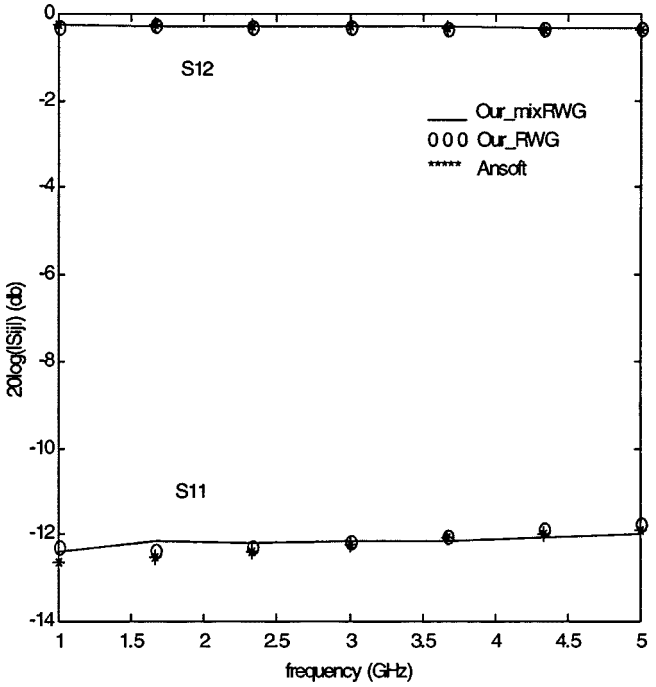

Fig. 8. Comparison of S-parameters obtained by the different basis functions. Ansoft Inc. uses triangle basis functions.

D. Test 4—Scattering by a 3-D Sphere

In this test, we compute the scattering of a 3-D perfect conducting sphere with the proposed basis functions of three different orders. Exact parametric representation of the sphere surface is used in the construction of the basis functions.

- We assume that the incident wave is a plane wave, i.e.,

$$\mathbf{E}^{\text{inc}}(\mathbf{r}) = E_0 \hat{x}\, e^{-j\mathbf{k}\cdot\mathbf{r}}$$

where $\hat{x}$ is the unit vector of the x-coordinate and $E_0 = 1.5$ and the propagation vector $\mathbf{k}$ is

$$\mathbf{k} = k\big(\sin\theta_0 \cos\varphi_0,\ \sin\theta_0 \sin\varphi_0,\ \cos\theta_0\big)$$

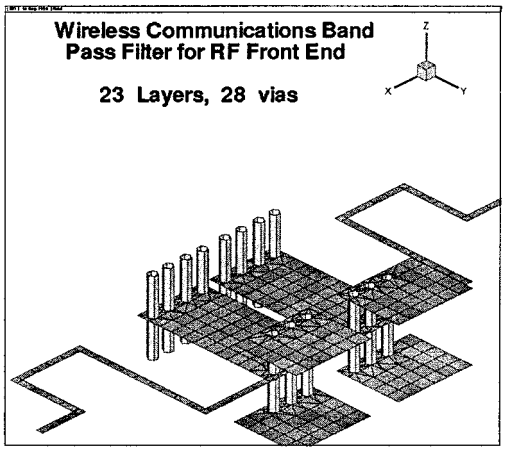

Fig. 9. Filter structure is discretized by a hybrid mesh.

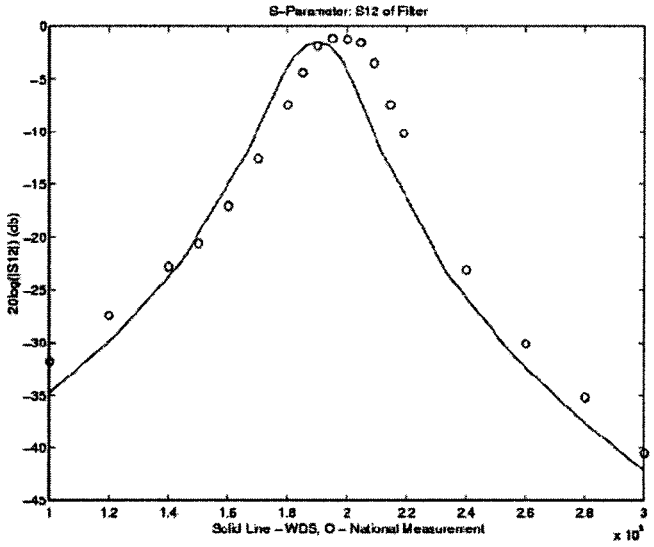

Fig. 10. Comparison of S_{12}-parameters of a bandpass filter, the unit for the horizontal axis is in hertz.

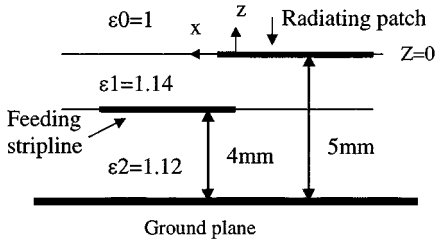

Fig. 11. Multilayer wide-band antenna.

with $\theta_0 = 0$. In our numerical test, the radius of the sphere is $a = (1/\pi)\lambda$, where wavelength $\lambda = (2\pi/k)$, $k = \omega\sqrt{\epsilon\mu}$, $\omega = 2\sqrt{2}$, the dielectric constant and permeability of medium are $\epsilon = 2\epsilon_0$, $\mu = \mu_0$ with ϵ_0, μ_0 being the dielectric constant and permeability of the vacuum, respectively.

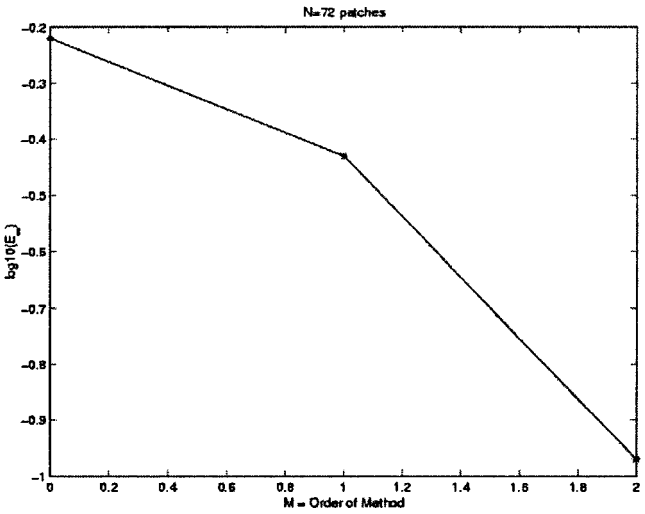

Fig. 12. $\log(E_\infty)$: maximum error E_∞ for current J_s over the sphere. Comparison of RWG, first and second-order methods ($N = 72$, top: $M = 0$, middle: $M = 1$, and bottom: $M = 2$. N is the number of edges of curved triangular patches, and M is the order of the basis functions).

The various computation parameters are as follows:

M order of the numerical methods, $M = 0$ denotes the original RWG basis;

N total number of edges of triangular patches of the sphere;

E_∞ maximum error for the surface currents, i.e.,

$$E_\infty = \max \|\mathbf{J}_{s,\,app} - \mathbf{J}_{s,\,ex}\|$$

where the maximum is taken over all triangle patches and $\mathbf{J}_{s,\,app}$ is the numerical solution and $\mathbf{J}_{s,\,ex}$ is the solution obtained by the mixed integral equation (MIE) series [20].

We compare the accuracy of RWG basis ($M = 0$), first-order method ($M = 1$), and second-order method ($M = 2$) with $N = 72$, their maximum error $\log(E_\infty)$ in the surface currents are -0.22, -0.43, and -0.97, respectively (see Fig. 12). There is much improvement of the maximum error as the order of the method is increased.

In a recent paper [21], we have addressed how to handle the singular integrals arising from the MOM so that high-order accuracy of the basis functions can be maintained.

V. Conclusion

We have demonstrated the flexibility and efficiency of using mixed high-order RWG basis functions in EM scattering with four applications. The combination of quadrilateral and triangular basis reduces the total number of unknowns in the impedance matrix. Higher order basis functions provide better accuracy for the same number of surface elements.

APPENDIX
HIGH-ORDER BASIS FUNCTIONS

A. Triangular and Triangular Patches Matching

The high-order basis function for a triangular and triangular patch in Fig. 4 can be written as

$$\mathbf{f}(\mathbf{x}) = \begin{cases} \dfrac{l}{\sqrt{g^+}}\Big(P_1^+(u_1, u_2)\partial_1\mathbf{x} + P_2^+(u_1, u_2)\partial_2\mathbf{x}\Big), \\ \qquad \text{if } \mathbf{x} = \mathbf{x}^+(u_1, u_2) \in T^+ \\ \dfrac{l}{\sqrt{g^-}}\Big(P_1^-(u_1, u_2)\partial_1\mathbf{x} + P_2^-(u_1, u_2)\partial_2\mathbf{x}\Big), \\ \qquad \text{if } \mathbf{x} = \mathbf{x}^-(u_1, u_2) \in T^- \end{cases}$$

where

$$\begin{aligned} &P_1^+(u_1, u_2) \\ &\quad = I_n^a g_A(u_1, u_2) + \sum_{m=2}^{M} \frac{I_n^{(m)} - \tilde{I}_t^{(m)}}{2} g_m^{e_2^+}(u_1, u_2) \\ &\qquad + \sum_{(l,m)\in\mathcal{L}_\Delta} c_{lm}^1 g_{lm}^{\text{int}} \\ &P_2^+(u_1, u_2) \\ &\quad = I_n^c g_C(u_1, u_2) + \sum_{m=2}^{M} \frac{I_n^{(m)} + \tilde{I}_t^{(m)}}{2} g_m^{e_2^+}(u_1, u_2) \\ &\qquad + \sum_{(l,m)\in\mathcal{L}_\Delta} c_{lm}^2 g_{lm}^{\text{int}} \end{aligned} \tag{30}$$

and

$$\begin{aligned} &P_1^-(u_1, u_2) \\ &\quad = -I_n^a g_A(u_1, u_2) + \sum_{m=2}^{M} \frac{-I_n^{(m)} - \hat{I}_t^{(m)}}{2} g_m^{e_2^-}(u_1, u_2) \\ &\qquad + \sum_{(l,m)\in\mathcal{L}_\Delta} d_{lm}^1 g_{lm}^{\text{int}} \\ &P_2^-(u_1, u_2) \\ &\quad = -I_n^c g_C(u_1, u_2) + \sum_{m=2}^{M} \frac{-I_n^{(m)} + \hat{I}_t^{(m)}}{2} g_m^{e_2^-}(u_1, u_2) \\ &\qquad + \sum_{(l,m)\in\mathcal{L}_\Delta} d_{lm}^2 g_{lm}^{\text{int}} \end{aligned} \tag{31}$$

with $e_2^- = e_2^+ = AC$

$$\mathcal{L}_\Delta = \Big\{(l, m),\, 0 \le l + m \le M - 3\Big\}. \tag{32}$$

Unknowns for each edge AC are

$$I_n^a,\, I_n^c,\, I_n^{(m)},\, \tilde{I}_t^{(m)},\, \hat{I}_t^{(m)}, \qquad 2 \le m \le M \tag{33}$$

and interior unknowns for each triangular patch are

$$c_{lm}^1,\, c_{lm}^2,\, d_{lm}^1,\, d_{lm}^2, \qquad (l, m) \in \mathcal{L}_\Delta. \tag{34}$$

B. Triangular and Quadrilateral Patches Matching

The high-order basis function for a triangular and quadrilateral patch in Fig. 5 can be written as

$$\mathbf{f}(\mathbf{x}) = \begin{cases} \dfrac{l}{\sqrt{g^\Omega}}\Big(Q_1(u_1, u_2)\partial_1\mathbf{x} + Q_2(u_1, u_2)\partial_2\mathbf{x}\Big), \\ \qquad \text{if } \mathbf{x} = \mathbf{x}_1(u_1, u_2) \in \Omega \\ -\dfrac{l}{\sqrt{g^T}}\Big(P_1(u_1, u_2)\partial_1\mathbf{x} + P_2(u_1, u_2)\partial_3\mathbf{x}\Big), \\ \qquad \text{if } \mathbf{x} = \mathbf{x}_2(u_1, u_2) \in T \end{cases} \tag{35}$$

where

$$\begin{aligned} &Q_1(u_1, u_2) \\ &\quad = I_n^b N_B(u_1, u_2) + I_n^c N_C(u_1, u_2) \\ &\qquad + \sum_{l=2}^{M} I_n^{(l)} N_l^{e_2}(u_1, u_2) + \sum_{2\le l,m\le M} \gamma_{lm}^1 N_{lm}^{\text{int}} \\ &Q_2(u_1, u_2) \\ &\quad = \sum_{l=2}^{M} \hat{I}_t^{(l)} N_l^{e_2}(u_1, u_2) + \sum_{2\le l,m\le M} \gamma_{lm}^2 N_{lm}^{\text{int}} \end{aligned} \tag{36}$$

$$\begin{aligned} &P_1(u_1, u_2) \\ &\quad = -I_n^b g_B(u_1, u_2) - \sum_{l=2}^{M} \frac{I_n^{(l)} - \tilde{I}_t^{(l)}}{2} g_l^{e_3'}(u_1, u_2) \\ &\qquad + \sum_{(l,m)\in\mathcal{L}_\Delta} c_{lm}^1 g_{lm}^{\text{int}} \\ &P_2(u_1, u_2) \\ &\quad = -I_n^c g_C(u_1, u_2) - \sum_{l=2}^{M} \frac{I_n^{(l)} + \tilde{I}_t^{(l)}}{2} g_l^{e_3'}(u_1, u_2) \\ &\qquad + \sum_{(l,m)\in\mathcal{L}_\Delta} c_{lm}^2 g_{lm}^{\text{int}} \end{aligned} \tag{37}$$

where $e_3' = e_2 = BC$. Also, the unknowns for each edge BC are

$$I_n^b,\, I_n^c,\, I_n^{(l)},\, \tilde{I}_t^{(l)},\, \hat{I}_t^{(l)}, \qquad 2 \le l \le M \tag{38}$$

and the interior unknowns for each triangular element are

$$c_{lm}^1,\, c_{lm}^2, \qquad (l, m) \in \mathcal{L}_\Delta \tag{39}$$

while the interior unknowns for each quadrilateral element are

$$\gamma_{lm}^1,\, \gamma_{lm}^2, \qquad 2 \le l, m \le M. \tag{40}$$

REFERENCES

[1] K. S. Yee, "Numerical solution of initial boundary value problems involving Maxwell equations in isotropic media," *IEEE Trans. Antennas Propagat.*, vol. AP-14, pp. 302–307, May 1966.

[2] J. R. Mosig, *Integral Equation Technique in Numerical Techniques for Microwave and Millimeter-Wave Passive Structure*, T. Itoh, Ed. New York: Wiley, 1989, pp. 133–213.

[3] R. F. Harrington, *Field Computation by Moment Methods*. New York: Macmillian, 1968.

[4] A. Sommerfeld, *Partial Differential Equations in Physics*. New York: Academic, 1964.

[5] W. Cai and T. Yu, "Fast calculation of dyadic Green's functions for electromagnetic scattering in a multi-layered medium," *J. Comput. Phys.*, vol. 165, pp. 1–21, 2000.

[6] Y. L. Chow, J. J. Yang, D. G. Fang, and G. E. Howard, "A closed-form spatial Green's function for the thick microstrip substrate," *IEEE Trans. Microwave Theory Tech.*, vol. 39, pp. 588–592, Mar. 1991.

[7] M. I. Aksun, "A robust approach for the derivation of closed-form Green's functions," *IEEE Trans. Microwave Theory Tech.*, vol. 44, pp. 651–658, May 1996.

[8] T. J. Cui and W. C. Chew, "Fast evaluation of Sommerfeld integrals for EM scattering and radiation by three dimensional buried objects," Univ. Illinois, Urbana-Champaign, IL, Res. Rep. CCEM-34-97, Dec. 1997.

[9] S. M. Rao, D. R. Wilton, and A. W. Glisson, "Electromagnetic scattering by surfaces of arbitrary shape," *IEEE Trans. Antennas Propagat.*, vol. AP-30, pp. 409–418, May 1982.

[10] S. Wandzura, "Electric current basis functions for curved surfaces," *Electromagnetics*, vol. 12, pp. 77–91, 1992.

[11] J. M. Song and W. C. Chew, "Moment method solutions using parametric geometry," *J. Electromag. Waves Applicat.*, vol. 9, no. 1/2, pp. 71–83, Jan.–Feb. 1995.

[12] M. I. Sancer, R. L. McClary, and K. J. Glover, "Electromagnetic computation using parametric geometry," *Electromagnetics*, vol. 10, no. 1–2, pp. 85–103, 1990.

[13] D. L. Wilkes and C.-C. Cha, "Method of moments solution with parametric curved triangular patches," in *IEEE AP-S Int. Symp. Dig.*, London, ON, Canada, 1991, pp. 1512–1515.

[14] W. Cai, "High order current basis functions for electromagnetic scattering of curved surfaces," *J. Sci. Comput.*, vol. 14, no. 1, pp. 73–107, 1999.

[15] W. C. Chew, *Waves and Fields in Inhomogeneous Media*, 2nd ed. Piscataway, NJ: IEEE Press, 1995.

[16] K. A. Michalski and D. Zheng, "Electromagnetic scattering and radiation by surfaces of arbitrary shape in layered media—Part I: Theory," *IEEE Trans. Antennas Propagat.*, vol. 38, pp. 335–344, Mar. 1990.

[17] J. R. Mantz and R. F. Harrington, "H-field, E-field and combined field solution for conducting bodies of revolution," *Arch. Elektr. Ubertragung*, vol. 32, pp. 157–164, Apr. 1978.

[18] B. Szabo and I. Babuska, *Finite Element Analysis*. New York: Wiley, 1991.

[19] J. C. Rautio, "A de-embedding algorithm for electromagnetics," *Int. J. Microwave Millimeter-Wave Computer-Aided Eng.*, vol. 1, pp. 282–287, 1991.

[20] R. F. Harrington, *Time Harmonic Electromagnetic Fields*. New York: McGraw-Hill, 1961.

[21] W. Cai, Y. J. Yu, and X. C. Yuan, "Singularity treatment and high order RWG basis functions for integral equations of electromagnetic scattering," *Int. J. Numer. Methods Eng.*, submitted for publication.

Wei Cai received the Ph.D. degree in applied mathematics from Brown University, Providence, RI, in 1989.

In 1989, he joined the Department of Mathematics, University of North Carolina, Charlotte, where he was an Assistant Professor. From 1994 to 1996, he was initially an Assistant Professor and then an Associate Professor in the Department of Mathematics, University of California at Santa Barbara. He is currently a Full Professor at the University of North Carolina. His research interest includes numerical combustion and computational electromagnetics. He is currently involved in the development of adaptive wavelet methods for flame propagations, and efficient numerical algorithms for EM scattering in layered media with applications for parameter extraction for computer packaging and very large scale integration (VLSI) simulations.

Tiejun Yu received the M.S. and Ph.D. degrees in electrical engineering from Tsinghua University, Beijing, China, in 1991 and 1996, respectively.

Prior to 1990, he was an Engineer in industry south of China. From 1991 to 1996, he was a Lecturer and an Assistant Professor in the Department of Electrical Engineering, Tsinghua University. In 1997, he joined the Department of Mathematics, University of North Carolina (UNC), Charlotte, as a Research Associate. In 1998, he joined the Department of Electrical Computer Engineering, Duke University, Durham, NC, where he was involved with demining research. In 2000, he joined the Cadence Company, San Jose, CA, where he is currently a Senior Research and Development Engineer. His current research interests include EM scattering, parameters extraction and simulation for ICs, VLSIs, and their packages.

Dr. Yu was the recipient of the 1998 Best Paper Award presented at the 35th Design Automation Conference (DAC).

Han Wang received the Ph.D. degree in computational mathematics from the Carnegie-Mellon University, Pittsburgh, PA, in 1996.

From 1996 to 1999, he was a Visiting Assistant Professor at the University of North Carolina, Charlotte. In 1999, he joined the Enovia Company, Charlotte, NC, 28262. He has been involved in the areas of computations of microstructures in material science, development of unstructured mesh generation algorithms, and computational EM fields.

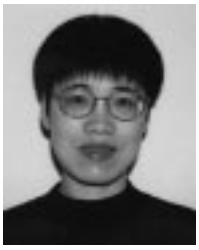

Yijun Yu is currently working toward the Ph.D. degree in applied mathematics at the University of North Carolina, Charlotte.

She is currently involved in the areas of computational EM-field and numerical-method theory.